Microbial single-cell omics in situ

Xihong Lan[1,2,3#], Qiaoxing Liang[1,2,3#], Jinhua He[4#], Jiayi Wu[1], Xiaoying Zhang[4], Fei Li[1,2,3], Guoping Zhao[1,2], Ruidong Guo[1], Lili Li[1], Huijue Jia[1,2,3]*

[1]Greater Bay Area Institute of Precision Medicine (Guangzhou), Fudan University, Guangzhou, China.

[2]School of Life Sciences, Fudan University, Shanghai, China.

[3]State Key Laboratory of Genetic Engineering, Fudan University, Shanghai, China.

[4]Central Laboratory of Panyu Central Hospital, The Affiliated Panyu Central Hospital of Guangzhou Medical University, Guangzhou, China.

[#]These authors contributed equally to this work.

*Corresponding author. Email: huijue_jia@fudan.edu.cn

Abstract

Metagenomics has enabled understanding of the microbial composition and functional potential in various environments. Using Laser-Induced Forward Transfer (LIFT) technology, we report high-quality microbial single-cell genome or transcriptome in complex samples such as saliva, mouse gut and human tumor sections. Neighboring cells could be separately retrieved and bacteria could be fluorescently labelled. We illustrate cell-fate commitment with sporulation. The method is scalable and precise, and would empower fundamental insight for microbial populations and single-cell interactions with the host.

Introduction

Single-cell transcriptome analyses for mammalian cells are reaching their prime, further boosted by spatial omics technology[1]. Single-cell omics for bacterial cells, however, have remained a daunting task, due to the orders of magnitude lower concentration of nucleic acids, the lack of a poly(A) tail, and the Poisson distribution of droplet microfluidics [2]. Marine cyanobacteria were among the first bacteria to be analyzed using single-cell genomes [3], due to their dominance in the global ocean. Single-cell genomes of extreme environments have revealed genomic features of uncultured bacteria and archaea [4]. Other than low-diversity communities, microbial single-cell studies have mostly been illustrated for model organisms such as *E. coli*, and the genome or transcriptome analyzed, often using targeted methods, has remained far from complete [5-9].

Laser-Induced Forward Transfer (LIFT) is a straight-forward way of manipulating microparticles including cells [10-13]. With a laser beam that

48 evaporates or deforms a thin metal coating[14, 15], LIFT is ideally suited for picking
49 particles in the size range of bacteria. It can potentially tolerate food particles,
50 cell debris, and other objects commonly present in the human microbiome that
51 could undermine analyses using droplet microfluidics.

52 Metagenomic analyses of low-biomass environment such as tumors and
53 placenta has been costly and controversial [16]. Thus, a direct approach to
54 characterize the microbes in tissues with over 99.9% host sequences would
55 also be very much welcomed.

56 Here we present microbial single-cell genomes and transcriptomes using
57 a commercially available optics equipment, and demonstrate their superb utility
58 in a number of scenarios.

59

60 ## Results

61 ### Draft genome quality assembly for microbial single cells

62 Consisted of several key modules[17], our LIFT equipment was capable of image
63 capture, Raman spectral acquisition and single cell isolation from complex
64 samples after previous processing steps (Sup. Fig. 1a-d; Sup Movies S1). Next,
65 we explored the energy and mode required for microbial cell ejection using
66 bacteria of different sizes and shapes. Low energy resulted in cell ejection
67 failure including cell shifting and cell rupture (Sup. Fig. 2a and b), while
68 appropriate energy for cell ejection successfully isolated the selected cell
69 without affecting the closely adjacent cells (Sup. Fig. 2c). Further separation of
70 cells with different morphological characters suggested that appropriate energy
71 for cell LIFT was related to the size of the cell rather than its shape (Sup. Fig.
72 2d). For the larger bacteria, multiple LIFT attempts could also successfully

separate the cells without increasing energy (Sup. Fig. 2e).

To develop microbial single-cell technology for complex samples, we started with saliva samples which are even more diverse than feces. A fresh saliva sample was centrifuged and spotted onto the slide (Sup. Fig. 1c), and bacteria cells were visualized before LIFT (Fig1.a). Single cells were ejected by LIFT without affecting neighboring cells (Fig1.a and b, no burnt circle with the low energy 60nJ) and Multiple Displacement Amplification (MDA) was performed in a PCR tube. Without the need for sophisticated algorithms to pool assembly from fragmental genomes, as was reported recently [5], here we used state-of-the-art algorithms developed for metagenomes [18], and obtained a bacterial genome of 99.99% completeness and low contamination 0.33% (Fig1.c, Sup. Fig. 3a-d). This genome was identified as *Megamonas funiformis*. Gene annotation through Bakta revealed the detection of coding sequences (CDSs), tRNAs, rRNAs, ncRNAs, and CRISPRs (Fig1.d, Table S1). Calculating the coding density showed that the genome sequence is >90% coding (Sup. Fig. 3e and f), which is within the range for commensal bacteria (on average 87% for human gut [19]). Thus, LIFT from complex samples could obtain high-quality single-cell bacteria genomes (single-cell assembled genomes, SAGs) that far exceeds typical single-cell genomes [5] or metagenomically assembled genomes [20], and are on-par with genomes from cultured isolates.

To validate the automatic process, *Sphingomonas sp000797515* labeled with TADA were precisely ejected from sparse regions and densely packed regions in mixture of several species, sequenced using two different reaction volume, both of which yielded high-quality genomes (Sup. Fig. 4a-d; Sup Movies S2). There were no significant differences in genome completeness,

98 contamination and coverage between the genomes obtained by the two
99 methods suggesting that downsizing the reaction volume does not lead to a
100 decline in SAGs quality (Sup. Fig. 4e). The single-cell genomes from LIFT were
101 also highly consistent (ANI>95%) with the known input genomes (Sup. Fig. 4f),
102 validating this approach.

103 To increase the throughput and eliminate individual differences in operation,
104 we made use of an automated pipetting platform to take over the molecular
105 biology work after automated single-cell ejection. With the aid of automatic
106 identification by adjusting parameters such as diameter, area and fluorescence
107 intensity, 34-62 bacteria from single strain suspensions and complex samples
108 could be precisely ejected within one minute for the next step of library
109 construction (Sup. Fig. 5a-c; Sup Movies S3-S4). Salivary microbes of three
110 fields from a single donor were marked for collection (0.1s per cell), which
111 consisted of diverse morphological characters (Fig2.a). After de novo assembly,
112 4 of the 39 SAGs have completeness >90 and contamination <5, which are
113 regarded as high quality [21]. 27 of the 39 SAGs have completeness >50 and
114 contamination <10, which are medium quality (Table S2). The species were
115 identified according to GTDB-Tk with ANI >95%. With this relatively small-scale
116 attempt, we already obtained oral bacteria from all major phyla, including
117 *Actinobacteriota*, *Bacteroidota*, *Campylobacterota*, *Firmicutes*, *Fusobacteriota*,
118 *Patescibacteria* and *Proteobacteria* (Fig.2b). Species from the oral cavity and
119 related body sites were seen, such as *TM7x*, *Haemophilus sp.*, *Neisserria sp.*,
120 *Porphyromonas gingivalis*, *Filifactor alocis*, *Fusobacterium peridonticum*,
121 *Bifidobacterium vaginale* (renamed from *Gardnerella vaginalis*) and
122 *Parabacteroides merdae* (Fig.2b). These results indicate that the single-cell

genomes could be reliably obtained with medium to high quality in an automated and selective manner to reveal the microbial landscape in a complex sample.

Cell-fate commitment revealed by single-cell transcriptome

Sporulation is a strategy for bacteria to survive harsh environments [22, 23], and to potentially distribute to other hosts. We cultured a strain of *Bacillus licheniformis* isolated from human saliva, and LIFT-picked single cells to analyze their transcriptome following citric acid treatment (Sup. Fig. 6a). Thousands of transcripts were detected from cells stimulated by citric acid (Sup. Fig. 6b), which is consistent with widespread yet incomplete expression of the bacterial genome per cell cycle, known for model organisms such as *E. coli* [24]. Besides protein coding genes, tRNAs and regulatory sRNAs were also detected (Sup. Fig. 6c), favoring the robustness of the experimental protocol.

In addition to scRNA analysis according to the bacteria reference genome (Sup. Fig. 6d-g), the high-quality reads obtained could also be de novo assembled. Gene counts obtained by these two analytical methods were similar (significance $p < 0.05$) and the expression profile was highly correlated (Sup. Fig. 6h). Thus, both known and unknown bacteria could be investigated using this scRNA approach.

Oligo(A) tails target bacterial mRNAs for degradation [25]; this coupling to exonucleases in bacteria is evolutionarily similar to exosome degradation of transcripts in the eukaryotic nucleus. We detected stretches of three or more adenylates in a number of transcripts (Sup. Fig. 7a-f, Table S3). TctA (Tripartite tricarboxylate transporter TctA family), a large transmembrane protein involved

148 in citrate uptake, for example, showed long stretches of poly(A) spanning the
149 entire gene, which led to three contigs in de novo assembly (Sup. Fig.7g and i).
150 The shorter form was more abundant in five of the five cells analyzed (Sup.
151 Fig.7h), consistent with degradation from 3' to 5'. These results highlight the
152 fundamental questions that can be addressed using high-quality microbial
153 single-cell transcriptome.

154 We next explored the dynamic transcription changes during the
155 commitment to sporulation in *B. licheniformis* following citric acid treatment. In
156 addition to the upright laser for LIFT, the commercially available equipment we
157 used also harbor an inverted laser for single-cell Raman spectrometry (Fig.3a).
158 Both the cell morphology and Raman spectra could be rapidly obtained from a
159 sample. During the citric acid-induced sporulation, the day 0, day 3 and day 9,
160 *B. licheniformis* cells can be visually and spectrally divided into three groups,
161 from day 0 rod (I), day 3 intermediate state (II) to day 9 oval spore (III) (Fig.3a
162 and b). The mean spectrum of cells I, II, III were different, and spectra from the
163 individual microbial cells formed three clusters (Fig.3c). Thus, the
164 morphological features of bacteria as well as Raman spectrum indicated
165 alterations in cellular gene expressions. Consistent with the decrease in growth,
166 while ribosomal RNAs, ribosomal proteins, and nucleoid associated proteins
167 dominated the day 0 transcriptome, the reads proportion of other genes notably
168 increased as the cells undergo morphological changes towards sporulation
169 (Sup. Fig. 8a). Comparison of the gene expression of cells I, II, III allowed us to
170 identify 194 differentially expressed genes, with these transcripts mainly
171 clustered into three groups according to variations in their reads counts (Fig.3d).
172 Gene ontology (GO) analysis of Biological Process (BP), Molecular Function

173 (MF), Cell Component (CC) showed that the genes preferentially expressed in
174 the intermediate state of group II are linked to the pathways such as cellular
175 response to stress, sporulation, hydrolase activity and intrinsic component of
176 membrane (Sup. Fig. 8b). Consistently, electron microscopy confirmed that
177 cellular component assembly occurred in cells II, which was also observed
178 before Raman microscopy and LIFT (Sup. Fig. 8c). Comparing cells I and cells
179 II, we found that germination gene *gerD* co-present with sporulation related
180 genes such as spore coat protein and *YjcZ* family sporulation protein were
181 upregulated after citric acid treatment at day 3 (Fig.3e). When cells I
182 transformed into spore, *spoIIIAC* (stage III sporulation protein AC), *YtvI*
183 (sporulation integral membrane protein) and spore-specific gene *splB* (spore
184 photoproduct lyase) were highly expressed (Fig.3f).

185 Further looking into the day 3 samples led to five types of cells with distinct
186 cell morphology, and the scRNA also formed five groups (Fig.4a). Principal
187 Component Analysis of gene expression profiles revealed that cells of type I,
188 type IV and type V were relatively clustered independently, while cells of type II
189 and type III were relatively dispersed (Fig.4b). Comparing gene counts in each
190 type, we found that cells of type II in cell division state were active in gene
191 transcription (Fig.4c). Genes whose expression were enriched in the different
192 cell types included enzymes, transcription regulator and biosynthesis proteins
193 (Fig.4d). Genes highly expressed in type I are FdhF/YdeP family
194 oxidoreductase, manA (mannose-6-phosphate isomerase, class I), PTS
195 mannose/fructose/sorbose transporter subunit IIC,
196 phosphoribosylaminoimidazolesuccinocarboxamide synthase, *ComGE* and 2-
197 dehydropantoate 2-reductase, which enable type I cells resistance to low PH

198 caused by citric acid, transporting sugar molecules, pantothenate biosynthesis,
199 DNA uptake and purine biosynthesis [26-30]. Genes highly expressed in type II
200 cells included DEAD/DEAH box helicase, primosomal protein DnaI, DNA
201 polymerase/3'-5' exonuclease PolX, DNA helicase RecQ, RNA-binding protein
202 and sigma-54-dependent Fis family transcriptional regulator, which indicated
203 DNA replication and gene transcription process in cell division [31, 32]. Genes
204 observed in type II were also expressed in type III, but relatively lower. When
205 cells changed into type IV, GTP associated genes MnmE, elongation factor Tu
206 and GTP 3',8-cyclase MoaA, 50S proteins and GntR family transcriptional
207 regulator were highly expressed, which regulated biological process such as
208 gene translation and cell motility [33, 34]. Genes in type V were mainly transporters,
209 Na+/H+ antiporter NhaC, permease and bacteriocin, which functioned in stress
210 resistance, substance exchange and inhibition of spore germination [35-37].
211 Comparing mean spectrum of five type cells, we observed Raman signal at
212 band 750nm-785nm contributed by Cytochrome c and metabolites of purine
213 degradation decreased (Fig.4e) [38, 39], which is consistent with variation of
214 metabolic and gene transcriptional activity in five type cells. In addition,
215 transcription of sporulation and spore related genes also varied with cell state
216 (Fig.4f). These results illustrate the discovery power of high-quality scRNA, and
217 indicate that visual and/or label-free Raman spectra-guided selection of
218 microbial single cells could greatly facilitate the investigation of heterogeneous
219 microbial populations. All cells could be rapidly scanned in seconds, before
220 more costly amplification and analyses.

221

222 **Single-cell microbial genome and transcriptome from tissue-resident**

223 **microbiota *in situ***

224 Having demonstrated single-cell draft genomes from complex samples and
225 high-quality precision single-cell transcriptome from heterogenous populations,
226 we went on to directly study microbial single-cells in tissue samples, which has
227 been impossible with other methods. After gavage of mice with Cy3-amino-D-
228 alanine (Cy3ADA) and Fam-amino-D-alanine (FADA), various morphologies of
229 fluorescent bacteria were observed in intestinal lavage fluid, indicating that
230 intestinal bacteria can be specifically labeled with amino-D-alanine (Fig.5a).
231 Therefore, we further observed fluorescent bacteria near the mucus of a mouse
232 colon and inside host cells (Fig.5b). Single bacteria could be extracted from
233 these regions either in a fluorescence-dependent or -independent manner
234 (Fig.5c and d). We selected 25 bacteria from three fields for genome
235 sequencing, obtaining 3 high-quality and 5 medium-quality SAGs. Among these
236 bacteria, there are typical mouse gut bacteria like *Prevotella copri A*,
237 *Escherichia flexneri*, *Turicimonas muris*, *Bacteroides intestinalis*, *Bacteroides*
238 *dorei* as well as more aerobic and peritoneal species such as *Cutibacterium*
239 *acnes*, *Staphylococcus capitis* (Fig.5e)[40, 41]. These results suggested that LIFT
240 could be applied to tissue samples.

241 We next applied the method to tumor samples from human patients.
242 Resected tumor tissues from a patient diagnosed as colorectal cancer (Sup.
243 Fig. 9a) were cut into tissue sections and loaded onto the slide for microbial
244 single-cell omics (Fig.6a). We confirmed cancer infiltrating and staging by
245 immunohistochemical staining of marker genes such as P53, BrafV600E, Ki67
246 (Sup.Fig.9b). Using antibodies against bacterial lipopolysaccharide (LPS) and
247 vancomycin to detect Gram-negative and Gram-positive bacteria respectively,

248 we observed microbes with diverse morphological features including rod shape
249 and spherical shape, distributed in colorectal cancer (Sup. Fig. 9c). Without
250 special treatment, we searched for microbes in the bright field. The microbes
251 have distinct Raman spectral fingerprints compared to histiocytic Raman
252 spectrum (Sup. Fig. 9d), which means this technology can very effectively avoid
253 sequencing of host cells or collection of non-microbial particles. For this
254 colorectal cancer sample, a 1.33μm long and rod-shaped single cell was
255 spotted and separated for genomic sequencing combined with Raman
256 spectrum acquisition (Fig.6b and c). We obtained a medium-quality SAG
257 identified as *Bacteroides intestinalis* based on Mash analysis (Fig.6d).
258 Phylogenetic analysis of all *B. intestinalis* genomes from metadata-gut of Mash
259 database and our SAG revealed that SAG was similar to MGYG000028343
260 which is also from China (Fig.6e).

261 Moreover, a rod-shaped single cell adhered to intestinal mucosal was
262 separated for RNA sequencing (Fig.7a). After removal of host gene reads, we
263 obtained de novo transcriptome assembly identified as *Bacteroides*
264 *xylanisolvens* by GTDB-Tk, in which 70% contigs and 75% transcripts (2756
265 transcripts) belonged to *Bacteroides* (Fig.7b). Of note, we observed dust
266 particles in the lungs of this colorectal cancer patient with 50 years of smoking
267 when cancer metastasized to the lungs (Sup. Fig. 10a and Sup. Fig. 10b), which
268 is consistent with the finding that *Bacteroides xylanisolvens* is involved in
269 nicotine degradation in smokers [42]. Among the ~3616 genes expressed were
270 nicotine-degrading gene nicX, membrane proteins SusC/RagA family TonB-
271 linked outer membrane protein, ABC transporter, sialic acid-specific
272 acetylesterase and porin (Fig.7c), which are crucial for nicotine degradation,

273 nutrients uptake and thrive of *Bacteroidetes* in the gut [43-45]. Gene ontology
274 analysis further verified that these genes were enriched in pathways of passive
275 transmembrane transporter activity, sialic acid transmembrane transporter
276 activity and porin activity (Fig.7d). These results suggest the application
277 potential of this method for tissue microbe detection *in situ* and single cell spatial
278 microbiome.

279

280 ## Discussion

281 Our study provides a method based on LIFT technique for cell isolation and
282 further high-quality single cell sequencing. This method can precisely and
283 automatically isolate individual bacteria from complex samples, either in a label-
284 dependent or label-free manner. After rapid automated sorting, the cells were
285 transferred to an automated platform for nucleic acid extraction and
286 amplification, in preparation for subsequent single-cell genome or
287 transcriptome sequencing to enhance throughput. We are positive that further
288 reducing the reaction volumes, optimizing the reagents, the plasticware and the
289 precision selection process will further demonstrate the advantage of this
290 single-cell omics approach that does not rely on microfluidics and exhaustive
291 sequencing of abundant cells.

292 Knowing the complete single-cell genome and transcriptome would be very
293 useful to understanding fundamental questions of the microbiome beyond
294 model organisms. Both the single-cell genome and the transcriptome could be
295 either reference-based or de novo assembled, the latter means applicability to
296 any new sample instead of a model bacterium. As is commonly seen for single-
297 cell studies of mammalian cells, merely increasing the number of cells

298 sequenced by a few fold would not necessary ensure identification of rare
299 populations. With our approach, rare populations could be enriched before
300 sequencing. Moreover, our method provided multidimensional information for
301 the study of single cell microbe, including bacterial shape, size, and Raman
302 spectrum. Visually, the existing software could already be set to select for cell
303 size, shape, area, etc (Sup. Fig.5b). Further standardization and algorithm
304 development for the single-cell Raman spectra would allow more precision in
305 sub-species analyses.

306 Another major advantage of this LIFT-based single-cell approach is that
307 complex samples require minimum pretreatment, and can contain other
308 particles or other cells. The separation of neighboring cells would also allow
309 elucidation of microscopic cooperation in a native environment in future studies.
310 We have previously reported multiple *Bacteroides* species in an Austrian cohort
311 of colorectal adenoma and carcinoma [46, 47] and *B. fragilis* were typically studied
312 in mice models of colitis [48]. Here the scRNA analyses have tentatively identified
313 metabolism of nicotine, mucin, etc. We have not yet tried FFPE samples, which
314 should be theoretically possible, so long as the nucleotides have not been too
315 degraded. Further application of our microbial single-cell omics method to
316 clinical samples would facilitate patient stratification and treatment.

317 In summary, here we present an optics-based strategy for precision single-
318 cell microbial genomics, and transcriptomes that could fully capture the
319 genomic landscape of host-associated microbiome, and allow nucleotide-
320 resolution understanding of microbial gene transcription and turnover in
321 individual cells in their native environment.

322 # Methods

323 ## Animals

324 Specific pathogen-free C57BL/6 mice (female, 8 weeks old) were purchased
325 from BESTEST Biotechnology Co., Ltd (Zhuhai, China) and maintained in the
326 laboratory Animal Center of Greater Bay Area Institute of Precision Medicine
327 (Guangzhou, China). These mice were bred in a temperature-controlled
328 environment (25℃, 12-hour light/dark cycle) with free access to food and clean
329 drinking water. All animal experiments were approved by the Animal Ethics
330 Committee at Greater Bay Area Institute of Precision Medicine and were
331 performed in accordance with guidelines approved by the Institutional Review
332 Board of Fudan University.

333

334 ## Study participants and sample collection

335 All the adult volunteers were not known to have chronic diseases, and did not
336 take antibiotics within the past three months. All healthy volunteers and the
337 patient had written informed consent. All the samples were self-collected into a
338 sterile tube, and handed in for further processing on the same day. The study
339 was approved by the Institutional Review Board of Fudan University. Tissue
340 collection was approved by the Ethics Committee at The Affiliated Panyu
341 Central Hospital of Guangzhou Medical University and was conducted following
342 guidelines established by this committee.

343

344 ## Laser Induced Forward Transfer (LIFT) of bacterial cells

345 The equipment, PRECI SCS-R300 (Hooke Instruments, Ltd., China), was
346 turned on and adjusted according to standards following the manufacturer's

347 handbook [49] (Sup. Movie 1). The optical setup is shown in Sup. Fig. 1. Laser
348 used for LIFT was nanosecond single pulse laser with 532nm wavelength, 5ns
349 pulse width and 3.4μJ energy, which could produce a single adjustable spot
350 capable of ejecting 0.5-20μm microorganisms. For complex shape and larger
351 microbes (greater than 20μm), LIFT combined with beam shaping could
352 successfully sort them. Laser for Raman spectral acquisition was continuous
353 laser with a maximum laser power of 50mW, 532nm wavelength. The
354 parameters of the laser for the acquisition of Raman spectra are set to 3mW,
355 3s.
356 The filtered and washed samples were spotted onto a quartz slide coated with
357 25nm thickness of aluminum film (HSC24, Hooke Instruments, Ltd.), and air-
358 dried in the hood. The Hooke chip was designed to incorporate a thermal
359 insulation structure to effectively protect the cell from heat-induced damage.
360 Visually selected bacterial cells (the manufacturer's software) were LIFT-
361 transferred into collectors (HSR04, Hooke Instruments, Ltd.) using a laser
362 energy below 75nJ (exceeding the minimum energy required by most microbes),
363 and then flipped into individual PCR tubes with brief spinning at 2000g (Yooning
364 Mini-6K).
365
366 **Whole genome amplification and sequencing from single bacterial cells**
367 Following cell lysis at 65℃ for 10 min, Multiple displacement amplification (MDA)
368 was performed using the REPLI-g scDNA Polymerase, according to kit
369 instructions (REPLI-g single cell kit, #150345, QIAGEN). Sequencing libraries
370 (PE150) were constructed without PCR, and sequenced on a DNBSEQ-T7
371 high-throughput sequencer (MGI).

372

373 **Genome assembly and analyses**

374 Quality control on paired-end sequencing reads of raw data was performed by
375 fastp (0.23.2) tool. The filtered reads were assembled by metaSPAdes (3.13.0)
376 in single cell mode. Based on binning information provided by Kraken2 (2.0.7),
377 the obtained assembled bins were processed with bin refinement using
378 BinSpreader. The quality of genome bins was analysed by Checkm2 and
379 QUAST. GTDB-Tk (1.0.2) was used to classify and taxonomically assign
380 genome bins. Phylogenetic trees were constructed by PhyloPhlAn (3.0.67) tool.

381

382 **Whole transcriptome amplification and sequencing from single bacterial**
383 **cells**

384 In addition to phosphate buffered saline (PBS) and lysis buffer according to the
385 QIAGEN kit (#150065), cell lysis was performed at 24℃ for 5 min, in the
386 presence of murine RNase Inhibitor (Vazyme), and MetaPolyzyme (MAC4L,
387 Invitrogen). Total RNA Reverse-transcription, ligation and MDA were performed
388 using the REPLI-g WTA single cell kit (#150065, QIAGEN), with extended
389 reaction time for bacteria instead of mammalian cells: 2 hours for ligation, 4
390 hours for MDA. Sequencing libraries (PE150) were constructed without PCR,
391 and sequenced on a DNBSEQ-T7 high-throughput sequencer (MGI).

392

393 **Single-cell transcriptome analyses**

394 For de novo transcriptome analysis, filtered reads of scRNA sequencing sample
395 was assembled using rnaSPAdes (3.15.5)[50]. Bakta (1.8.1) conducts a
396 comprehensive annotation of assembled transcriptome. Protein sequences

397 generated by Bakta (version 1.8.1; AMRFinderPlus for AMR gene annotations;
398 a generalized protein sequence expert system for identity, distinct coverage and
399 identity and priority values for each sequence) were further annotated by
400 eggnog-mapper (5.0.2) for gene function. KofamScan is used to annotate
401 protein sequences with KEGG Orthology (KO). DeepFRI is used to predict
402 Enzyme Commission (EC) numbers and Gene Ontology (GO) terms for Bakta
403 annotated genes. For analyzing the distribution and characteristics of oligoA,
404 bioawk tool is used to analyze oligoA positions in gene/contig level, and then
405 process the results to obtain matrix containing gene/contig lengths, oligoA
406 positions, gene start and gene end positions. All transcripts in de novo
407 transcriptome were evenly divided into ten percentile according to gene length
408 and the number of occurrences of oligoA positions within each percentile range
409 of the gene lengths was recorded. Standard deviation of oligoA distribution was
410 calculated according to the fraction of counts in each percentile range of the
411 gene length. The proportion of oligoA occurrence was normalized by R package
412 “Mfuzz”. The analysis of poly(A) with nine adenylate residues (9A) or more
413 followed these steps. Bowtie2 is used to align reads to transcripts and calculate
414 gene FPKM values. For genome-based analysis, reads are referred against
415 *Bacillus licheniformis* genome and genome annotation GTF file
416 (GCF_002074095.1) downloaded from NCBI database. After alignment with
417 Bowtie2, gene quantification was performed using featureCount (subread2.0.3).
418 Genes expression with fold change ≥1.5 and pvalue < 0.05 were determined as
419 significant change using DESeq2 (version 1.20.0). Gene enrichment of
420 Biological Process (BP), Molecular Function (MF), Cell Component (CC) was
421 analysed by R package Clusterprofiler with pvalueCutoff = 0.05. Heatmaps of

422 gene expression were using R package “pheatmap”. The bar plots, bubble plots
423 of GO analysis, scatterplots, and boxplots were visualized using on-line tool
424 imageGP (http://www.ehbio.com/ImageGP/index.php/Home/Index/index.html).
425

426 ***Bacillus licheniformis* culture and transmission electron microscopy**

427 The stored *Bacillus licheniformis* strain was inoculated into the Columbia Broth
428 medium overnight at 37°C. 100μl *Bacillus licheniformis* suspension was
429 transferred to 2ml medium containing 10% Columbia Broth, in which PH was
430 adjusted to 4.0 by adding citric acid. *Bacillus licheniformis* were cultured in citric
431 acid-amended 10% Columbia Broth for day 3 (exhibited a variety of
432 morphologies) and day 9 (almost all transformed into spore at day 9). Then
433 *Bacillus licheniformis* suspension was passed through 40μm cell strainers to
434 eliminate cell clumps. The resulting filtrate was centrifuged at 12,000g for 3
435 minutes to collect bacterial pellets. These pellets were then washed three times
436 with 1.5 ml of PBS each and finally resuspended in 0.7ml ddH2O. Prior to using
437 PRECI SCS R300 devices, 1-2 μl of the cell suspension was dropped onto chip
438 and allowed to dry either by evaporation at room temperature or by exposure
439 to sterile airflow in a biosafety cabinet.

440 For transmission electron microscopy, citric acid treated *Bacillus*
441 *licheniformis* were fixed with 4% PFA and stored at 4℃. The copper mesh was
442 incubated in 10μl fixed *Bacillus licheniformis* solution for 2 minutes. After
443 removal of excessive solution using filter paper, copper mesh was incubated
444 with 1% phosphotungstic acid (PTA) for 2 minutes and observed by electron
445 microscope (FEI Tecnai G2 spirit).
446

447 **Metabolic labeling with fluorescent D-alanine in culture**

448 TADA (tetramethylrhodamine-amino-D-alanine), Cy3ADA (Cyanine3-amino-D-
449 alanine) and FamADA (5-Carboxyfluorescein-amino-D-alanine) were
450 purchased from GuoPing Pharmaceutical (Anhui province, China).
451 *Staphylococcus capitis*, *Streptococcus oralis*, *Lactobacillus plantarum*,
452 *Akkermansia muciniphila* and *Clostridium butyricum* were isolated from faeces,
453 urine and saliva using our LIFT technology and cultured in Gifu Anaerobic
454 Medium at anaerobic incubator. The *Sphingomonas sp000797515* were
455 generously provided by HOOKE Instruments Ltd. The *Sphingomonas*
456 *sp000797515* were cultured in Luria-Bertani Medium and incubated with TADA
457 probes (40mM) at 37℃ for 3 hours. After incubation, the *Sphingomonas*
458 *sp000797515* were washed with PBS thrice, and mixed with other single-strain
459 bacteria in ddH2O for the following analyses. The *Sphingomonas sp000797515*
460 genome provided was assembled from our single strain suspension
461 sequencing.

462

463 **Metabolic labeling with fluorescent D-alanine in mice**

464 Cy3ADA and FamADA were administered to mice via gavage to label
465 mouse gut microbiota. In brief, Mice were gavaged with Cy3ADA and FamADA
466 probes dissolved in 200μl of PBS at 1 mM concentration. 6 hours later, Mice
467 were anesthetized using sodium pentobarbital (50 mg/kg). A part of mouse
468 large intestine was excised and minced using scissors in 2ml of PBS buffer.
469 Subsequently, the minced tissue was passed through 40μm cell strainers to
470 eliminate nonbacterial tissues and food debris. The resulting filtrate was
471 centrifuged at 12,000g for 3 minutes to collect bacterial pellets. These pellets

472 were then washed three times with 1.5ml of PBS each and finally resuspended
473 in ddH2O. The bacterial suspension was placed under a Leica fluorescence
474 microscope (ECLIPSE Ni-U) to observe the labeling of the bacteria.
475
476 **Tissue pretreatment for LIFT cell sorting and Hematoxylin-Eosin staining,**
477 **Immunofluorescence staining, Gomoris staining**
478 After euthanizing the mice, a small segment of colon tissue (0.5-0.8cm length)
479 free of food debris was excised, embedded in OCT (optimal cutting temperature
480 compound), and frozen. The frozen colon tissue was sectioned into slices with
481 6μm thickness and mounted flat onto glass slides and LIFT chip.
482 Several pieces of 2mm thickness tissues (20×20×2mm) separated by
483 laparoscopic colorectal cancer surgery were placed on filter paper and dry
484 gauze pad. After removal of excessive water, tissues were transferred to
485 supporter of freezing microtome (Leica CM1860 UV) and embedded with OCT.
486 In order to ensure the operation of the tissue section, OCT embedded tissue
487 was placed on cryo-stage until it's a solid ice cube. Processed tissue was
488 sectioned into 7μm thickness for Raman spectrometry and LIFT on PRECI
489 SCS-R300 (Hooke Instruments, Ltd., China) with 75nJ laser energy.
490 Dehydrated and paraffin embedded tissues were cut into 5μm thickness
491 and were stained with hematoxylin-eosin after de-paraffinization. For
492 immunofluorescence staining, tissue sections were treated with antigen
493 retrieval buffers, and then permeabilized and blocked by mixed solution of 0.3%
494 Triton X-100 and 5% BSA for 1 hour. Primary antibodies were used to incubate
495 tissue sections overnight at 4°C. Phosphate Buffer Saline containing 0.1%
496 Tween-20 (PBST) was used to wash tissue sections five times. Well-washed

sections were carefully incubated with secondary antibodies for 1 hour at room temperature. DAPI (4',6-diamidino-2-phenylindole) diluted at PBS with concentration 1:1000 was used to cell nuclei staining. Immunofluorescence images were captured by Leica sp8 system. Antibodies and their working concentration are listed as followed: anti-CK20 (ZSGB-BIO, #ZA-0574, 1:200), CDX2 (ZSGB-BIO, #ZA-0520, 1:200), Villin (ZSGB-BIO, #ZA-0575, 1:300), MSH2 (ZSGB-BIO, #ZA-0622, 1:250), MSH6 (ZSGB-BIO, #ZM-0367, 1:250), MLH1 (ZSGB-BIO, #ZM-0152, 1:300), PMS2 (ZSGB-BIO, #ZA-0542, 1:200), P53 (ZSGB-BIO, #ZM-0408, 1:200), BrafV600E (Roche, #760-5095, 1:300), and Ki67 (ZSGB-BIO, #ZM-0166, 1:300), anti-LPS (Cloud-Clone, #MAB526Ge22, 1:150), anti-Vancomycin (Invitrogen, #V34850, 1:150).

Gomoris staining method followed the manufacturer's protocol (Baso diagnostics. Inc. Zhuhai. China, #BA4375A). Briefly, 5μm thickness paraffin tissue sections were brought to water via xylene and descending grades of ethanol for deparaffinization. Following nuclear staining by Weigert's Iron Hematoxylin, sections were placed in Solution A for 15 minutes. After rinsing off the stain with distilled water, sections were stained with Solution B. After dehydration with ethanol and clearing with xylene, sections were mounted with a resinous medium.

References

1. Stahl, P.L. et al. Visualization and analysis of gene expression in tissue sections by spatial transcriptomics. *Science* **353**, 78-82 (2016).
2. Kuchina, A. et al. Microbial single-cell RNA sequencing by split-pool barcoding. *Science* **371** (2021).
3. Kashtan, N. et al. Single-cell genomics reveals hundreds of coexisting subpopulations in wild Prochlorococcus. *Science* **344**, 416-420 (2014).
4. Rinke, C. et al. Insights into the phylogeny and coding potential of microbial dark matter. *Nature* **499**, 431-437 (2013).
5. Zheng, W. et al. High-throughput, single-microbe genomics with strain

resolution, applied to a human gut microbiome. *Science* **376**, eabm1483 (2022).
6. Dar, D., Dar, N., Cai, L. & Newman, D.K. Spatial transcriptomics of planktonic and sessile bacterial populations at single-cell resolution. *Science* **373** (2021).
7. Pountain, A.W. et al. Transcription-replication interactions reveal bacterial genome regulation. *Nature* **626**, 661-669 (2024).
8. Lan, F. et al. Massively parallel single-cell sequencing of diverse microbial populations. *Nat Methods* **21**, 228-235 (2024).
9. Ma, P. et al. Bacterial droplet-based single-cell RNA-seq reveals antibiotic-associated heterogeneous cellular states. *Cell* **186**, 877-891 e814 (2023).
10. Florian, C. & Serra, P. Printing via Laser-Induced Forward Transfer and the Future of Digital Manufacturing. *Materials (Basel)* **16** (2023).
11. Barron, J.A., Krizman, D.B. & Ringeisen, B.R. Laser printing of single cells: statistical analysis, cell viability, and stress. *Ann Biomed Eng* **33**, 121-130 (2005).
12. Karakaidos, P., Kryou, C., Simigdala, N., Klinakis, A. & Zergioti, I. Laser Bioprinting of Cells Using UV and Visible Wavelengths: A Comparative DNA Damage Study. *Bioengineering (Basel)* **9** (2022).
13. Kryou, C. & Zergioti, I. Laser-Induced Forward Transfer on Regenerative Medicine Applications. *Biomedical Materials & Devices* **1**, 5-20 (2022).
14. Deng, Y., Renaud, P., Guo, Z., Huang, Z. & Chen, Y. Single cell isolation process with laser induced forward transfer. *J Biol Eng* **11**, 2 (2017).
15. Ye, K. et al. Spatial transcriptomic profiling of isolated microregions in tissue sections utilizing laser-induced forward transfer. *PLoS One* **19**, e0305977 (2024).
16. Jia H. Investigating Human Diseases with the Microbiome. (Elsevier, ed. 1st, 2022, https://www.elsevier.com/books/investigating-human-diseases-with-the-microbiome/jia/978-0-323-91369-0) (2022).
17. 梁鹏. 基于激光诱导向前转移的微生物单细胞弹射分选技术研究. 中国科学院大学(长春光学精密机械与物理研究所). (2022).
18. Meyer, F. et al. Critical Assessment of Metagenome Interpretation: the second round of challenges. *Nat Methods* **19**, 429-440 (2022).
19. Li, J. et al. An integrated catalog of reference genes in the human gut microbiome. *Nat Biotechnol* **32**, 834-841 (2014).
20. Zhu, J. et al. Over 50,000 Metagenomically Assembled Draft Genomes for the Human Oral Microbiome Reveal New Taxa. *Genomics Proteomics Bioinformatics* **20**, 246-259 (2022).
21. Bowers, R.M. et al. Minimum information about a single amplified genome (MISAG) and a metagenome-assembled genome (MIMAG) of bacteria and archaea. *Nat Biotechnol* **35**, 725-731 (2017).
22. Greene, R.A. & Slepecky, R.A. Minimal requirements for commitment to sporulation in Bacillus megaterium. *J Bacteriol* **111**, 557-565 (1972).
23. Schultz, D., Wolynes, P.G., Ben Jacob, E. & Onuchic, J.N. Deciding fate in adverse times: sporulation and competence in Bacillus subtilis. *Proc Natl Acad Sci U S A* **106**, 21027-21034 (2009).
24. Macklin, D.N. et al. Simultaneous cross-evaluation of heterogeneous E. coli datasets via mechanistic simulation. *Science* **369** (2020).
25. Bandyra, K.J. & Luisi, B.F. Licensing and due process in the turnover of bacterial RNA. *RNA Biol* **10**, 627-635 (2013).
26. Iobbi-Nivol, C. & Leimkuhler, S. Molybdenum enzymes, their maturation and molybdenum cofactor biosynthesis in Escherichia coli. *Biochim Biophys Acta* **1827**, 1086-1101 (2013).
27. McCoy, J.G., Levin, E.J. & Zhou, M. Structural insight into the PTS sugar

580 transporter EIIC. *Biochim Biophys Acta* **1850**, 577-585 (2015).
581 28. Price, D.R. & Wilson, A.C. A substrate ambiguous enzyme facilitates genome
582 reduction in an intracellular symbiont. *BMC Biol* **12**, 110 (2014).
583 29. Mom, J., Chouikha, I., Valette, O., Pieulle, L. & Pelicic, V. Systematic
584 functional analysis of the Com pilus in Streptococcus sanguinis: a
585 minimalistic type 4 filament dedicated to DNA uptake in monoderm bacteria.
586 *mBio* **15**, e0266723 (2024).
587 30. Levdikov, V.M. et al. The structure of SAICAR synthase: an enzyme in the de
588 novo pathway of purine nucleotide biosynthesis. *Structure* **6**, 363-376 (1998).
589 31. Bruand, C., Farache, M., McGovern, S., Ehrlich, S.D. & Polard, P. DnaB, DnaD
590 and DnaI proteins are components of the Bacillus subtilis replication restart
591 primosome. *Mol Microbiol* **42**, 245-255 (2001).
592 32. Shingler, V. Signal sensing by sigma 54-dependent regulators: derepression
593 as a control mechanism. *Mol Microbiol* **19**, 409-416 (1996).
594 33. Ramakrishnan, V. Ribosome structure and the mechanism of translation. *Cell*
595 **108**, 557-572 (2002).
596 34. Liu, G.F., Wang, X.X., Su, H.Z. & Lu, G.T. Progress on the GntR family
597 transcription regulators in bacteria. *Yi Chuan* **43**, 66-73 (2021).
598 35. Jack, D.L., Yang, N.M. & Saier, M.H., Jr. The drug/metabolite transporter
599 superfamily. *Eur J Biochem* **268**, 3620-3639 (2001).
600 36. Zhang, R. et al. A Novel MFS-MDR Transporter, MdrP, Employs D223 as a Key
601 Determinant in the Na(+) Translocation Coupled to Norfloxacin Efflux. *Front*
602 *Microbiol* **11**, 955 (2020).
603 37. Egan, K. et al. Bacteriocins: Novel Solutions to Age Old Spore-Related
604 Problems? *Front Microbiol* **7**, 461 (2016).
605 38. Premasiri, W.R. et al. The biochemical origins of the surface-enhanced Raman
606 spectra of bacteria: a metabolomics profiling by SERS. *Anal Bioanal Chem* **408**,
607 4631-4647 (2016).
608 39. Kaila, V.R.I. & Wikstrom, M. Architecture of bacterial respiratory chains.
609 *Nat Rev Microbiol* **19**, 319-330 (2021).
610 40. Xiao, L. et al. A catalog of the mouse gut metagenome. *Nat Biotechnol* **33**,
611 1103-1108 (2015).
612 41. Liu, L. et al. Rotenone Induces Parkinsonism with Constipation Symptoms in
613 Mice by Disrupting the Gut Microecosystem, Inhibiting the PI3K-AKT Signaling
614 Pathway and Gastrointestinal Motility. *Int J Mol Sci* **26** (2025).
615 42. Chen, B. et al. Gut bacteria alleviate smoking-related NASH by degrading gut
616 nicotine. *Nature* **610**, 562-568 (2022).
617 43. Robinson, L.S., Lewis, W.G. & Lewis, A.L. The sialate O-acetylesterase EstA
618 from gut Bacteroidetes species enables sialidase-mediated cross-species
619 foraging of 9-O-acetylated sialoglycans. *J Biol Chem* **292**, 11861-11872 (2017).
620 44. Papamichail, D. & Delihas, N. Outer membrane protein genes and their small
621 non-coding RNA regulator genes in Photorhabdus luminescens. *Biol Direct* **1**,
622 12 (2006).
623 45. Hall, L.M. et al. Sequence diversity and antigenic variation at the rag locus
624 of Porphyromonas gingivalis. *Infect Immun* **73**, 4253-4262 (2005).
625 46. Feng, Q. et al. Gut microbiome development along the colorectal adenoma-
626 carcinoma sequence. *Nat Commun* **6**, 6528 (2015).
627 47. Wang, J. & Jia, H. Metagenome-wide association studies: fine-mining the
628 microbiome. *Nat Rev Microbiol* **14**, 508-522 (2016).
629 48. Wong, C.C. & Yu, J. Gut microbiota in colorectal cancer development and
630 therapy. *Nat Rev Clin Oncol* **20**, 429-452 (2023).
631 49. Instruments, H. PRECI SCS-R300 Raman Single Cell Sorter. (https://www.hooke-
632 instruments.com/ProductCenter/). (2022).

50. Bushmanova, E., Antipov, D., Lapidus, A. & Prjibelski, A.D. rnaSPAdes: a de novo transcriptome assembler and its application to RNA-Seq data. *Gigascience* 8 (2019).

Acknowledgements

The authors were grateful to Zhong Yang, Lili Li, Jiong Ma, Xu Zhang, Hang Li, Meiya Lin for equipment support. Ping Sun, Miaoyi Kuang for sequencing support. We thanked Prof. Hao Chen (Shanghai Institute of Materia Medica, Chinese Academy of Sciences) and Prof. Xin Feng (Jilin University) for their suggestions on mouse gut microbiota labeling.

Author contributions

Xihong Lan and Huijue Jia conceived and designed the methodology; Xihong Lan developed and performed the experiments with assistance from Jiayi Wu; Xihong Lan and Jiayi Wu optimized sequencing library preparation; Jinhua He and Xiaoying Zhang prepared tissue sections; Xihong Lan, Qiaoxing Liang and Ruidong Guo performed the sequencing data analysis; Xihong Lan wrote the original manuscript; Huijue Jia and Guoping Zhao revised the manuscript; Huijue Jia supervised the study.

Competing interests

H.J. was a shareholder of MGITech Inc. The remaining authors declare no competing interests.

Correspondence and requests for materials

Further information and requests for resources and reagents should be directed to and will be fulfilled by the lead contact: Huijue Jia (huijue_jia@fudan.edu.cn)

Figure captions

Figure.1 High-quality microbial single-cell draft genome obtained from saliva. (a) A view of the sample before and after ejection of the selected microbial cell. A single cell as indicated was selected for genomic sequencing. Scale bar 10μm. **(b)** Diagram illustrating the imaging by the inverted microscope and LIFT by the upright microscope, on the commercially available PRECI-SCS equipment. The collectors are placed on a wheel, whose rotation is controlled by the manufacturer's software (Multiple cells could also be transferred into the same collector, depending on the experimental design). **(c)** Visualization of single-cell assembled genome by CGView tool displaying GC skew, feature labels, GC content, divider rings, and tick density. **(d)** The pie chart of single-cell assembled genome annotation display different categories including coding sequence (CDS), CRISPR, ncRNA region, ncRNA, replication origin (oriC), rRNA, tetracycline resistance, tRNA with their respective proportions.

Figure.2 Automated microbial single-cell genomics. (a) Individual microbial cells of saliva distributed on the chip were observed before LIFT. The selected microbes numerically marked with variable morphology are ejected for single cell sequencing. Scale bar, 10μm. **(b)** A phylogeny constructed from 39 obtained SAGs genome sequence is represented by the inner dendrogram. The phylum of each SAGs is indicated by the branch color. Numbers for the tip nodes of the dendrogram are corresponding to numbers labeled in panel. Completeness and contamination of each SAGs are represented by two heatmaps overlay on the phylogenetic tree. The species name of each SAGs is listed in the outermost ring.

Figure.3 Coherent grouping of *B. licheniformis* cells visually, spectrally and with scRNA transcriptome. (a) Individual *B. licheniformis* cells I (treated without citric acid), II (treated with citric acid for 3 days), III (treated with citric acid for 9 days) distributed on the chip were observed in bright field before Raman spectrometry and LIFT. Scale bar, 10μm. **(b)** More than 50 cells from each group (Cells I, Cells II and Cells III) are selected for Raman spectra acquisition. Dimensionality reduction is performed on the obtained Raman spectra by UMAP. **(c)** The means and standard deviations of Raman spectra were calculated for each group. **(d)** *B. licheniformis* of morphological forms I (treated without citric acid), II (treated with citric acid for 3 days) and III (treated with citric acid for 3 days) were ejected (two cells for each group) for scRNA sequencing. Heatmap of differentially expressed transcripts in Cells I, Cells II and Cells III. The candidate transcripts are mainly clustered into three groups (left panel). Violin plot of normalized transcripts expression in Group I, Group II and Group III (right panel). Data are represented as mean ± SE (ns: $P > 0.05$, $^{*}P < 0.05$, $^{**}P < 0.01$, $^{***}P < 0.001$) and calculated using ANOVA with post-hoc Tukey HSD Test. **(e)** Volcano plot of differentially expressed genes of Cells II

versus Cells I. Gene counts normalized and compared by DeSeq2. **(f)** Volcano plot of differentially expressed genes of Cells III versus Cells I. Gene counts normalized and compared by DeSeq2.

Figure.4 Single-cell transcriptome reveal heterogeneity in sporulation. (**a**) Image of five type (four cells for each type) *B. licheniformis* cells in sample treated with citric acid for 3 days and cells without citric acid treatment as control. Scale bar, 1μm. (**b**) Principal Component Analysis of gene expression profile from the five cell types. **(c)** Calculation of gene counts in each cell type. Data are represented as mean ± SE (*P < 0.05, **P < 0.01, ***P < 0.001) and calculated using two-tailed unpaired Student's t-test. **(d)** Heatmap of representative gene expression (z-score of log-transformed values) from 20 individual *B. licheniformis* cells grown in day 3 citric acid-treated media. (**e**) Raman spectra of five type *B. licheniformis* cells. The spectra are averages of ten individual spectra and normalized to the intensity of the strongest feature in each spectrum. **(f)** Dot plot of genes involved in *B. licheniformis* sporulation. Gene expression and pvalue were calculated between the selected cell type and the remaining cell type.

Figure.5 LIFT ejection of bacteria in mouse gut in bright and fluorescent field. (a) Representative images of bacterial morphology in mouse large intestinal lavage suspension after gavage with Cy3-ADA in mice. Scale bar, 10μm. **(b)** Cy3-ADA and Fam-ADA labeled bacteria on mouse large intestine sections. Scale bar, 100μm. **(c)** Localized composite image of mouse large intestinal tissue sections (upper panel). Scale bar, 200μm; LIFT ejection of bacteria on mouse large intestine sections in bright field (lower panel). Scale bar, 10μm. **(d)** LIFT ejection of bacteria on mouse large intestine sections in fluorescent field. Scale bar, 10μm. **(e)** 25 single bacteria were isolated from three fields of view in the mouse large intestinal tissue sections. A phylogeny constructed from 25 obtained SAGs genome is represented by the inner dendrogram. The phylum of each SAGs is indicated by the branch color. Completeness and contamination of each SAGs are represented by two heatmaps overlay on the phylogenetic tree. The species name of each SAGs is listed in the outermost ring.

Figure.6 Genomic sequencing for single microbe in tissue. (a) Diagram for the colorectal cancer sample. **(b)** Tissue section containing the microbial single-cell ejected and genome sequenced. Scale bar, 10μm. **(c)** Raman spectrum of the indicated single cell. **(d)** Visualization of obtained SAG (bin Bacteroides) by CGView tool displaying GC skew, feature labels, GC content, divider rings, and tick density. **(e)** Phylogenetic tree was constructed by obtained SAG (bin Bacteroides) and all *Bacteroides intestinalis* genomes downloaded from metadata-gut of Mash database. Among Bacteroides intestinalis genomes from Mash database, genome *MGYG000028343* was isolated from China.

748

749 **Figure.7 Transcriptome sequencing for single microbes from tissue. (a)**
750 Tissue section as in Figure 6, with inlets indicating the position of the bacteria
751 for scRNA analyses. Scale bar, 10μm. **(b)** Count ratio of contigs, transcripts in
752 single cell assembled transcriptome and genes by genome-based analysis.
753 Contig classification was annotated by Kraken2. Transcript annotation was
754 referred against de novo transcriptome annotated by eggnog-mapper software.
755 Gene annotation was referred against *Bacteroides xylanisolvens* genome (total
756 5306 genes). **(c)** The detection of nicotine degradation gene nicX and proteins
757 located on cell membrane. Gene FPKM was calculated by Bakta. **(d)** Gene
758 ontology analysis of transcripts classified to *Bacteroidetes*.

Fig.1

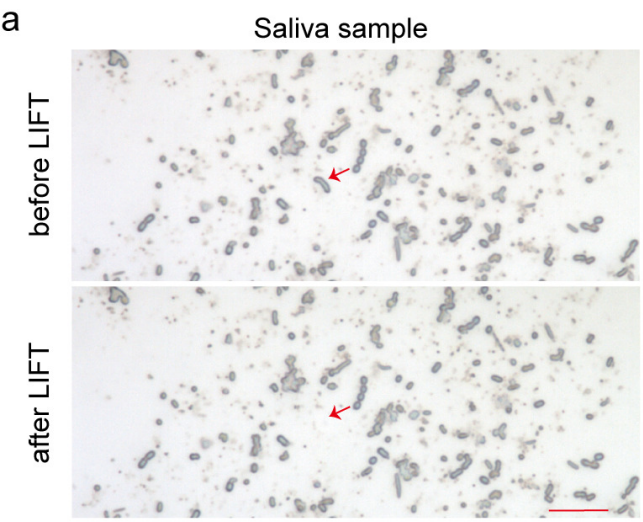
a
Saliva sample
before LIFT
after LIFT

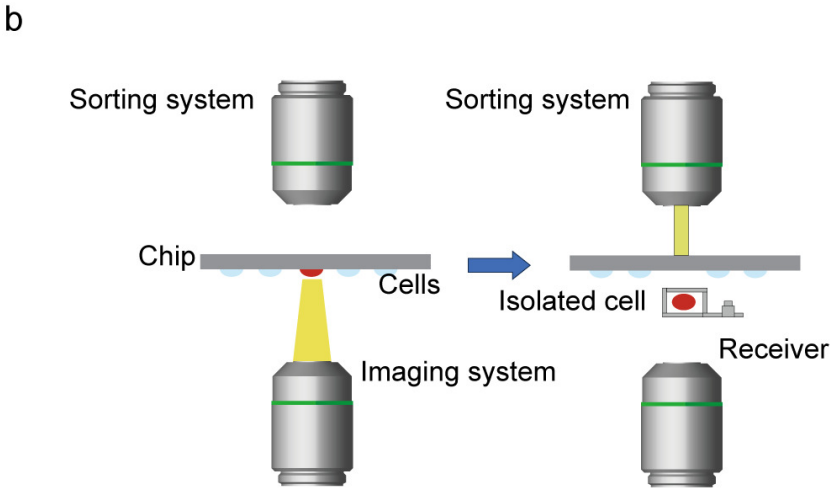
b
Sorting system
Sorting system
Chip
Cells
Isolated cell
Imaging system
Receiver

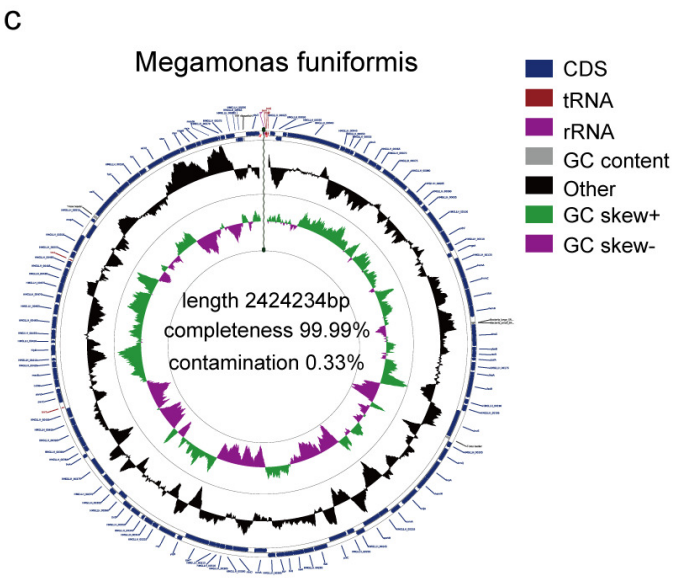
c
Megamonas funiformis
CDS
tRNA
rRNA
GC content
Other
GC skew+
GC skew-
length 2424234bp
completeness 99.99%
contamination 0.33%

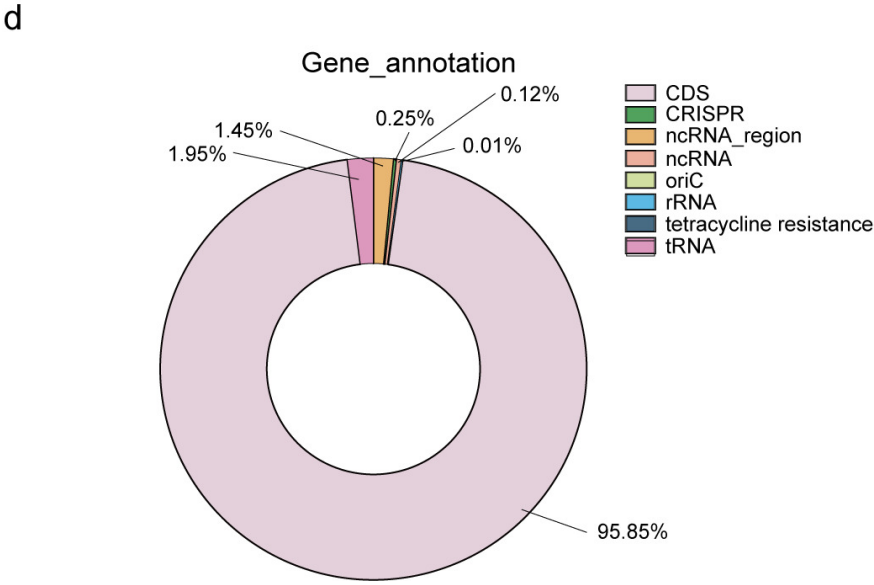
d
Gene_annotation
0.12%
0.25%
1.45%
1.95%
0.01%
95.85%
CDS
CRISPR
ncRNA_region
ncRNA
oriC
rRNA
tetracycline resistance
tRNA

Fig.2

a

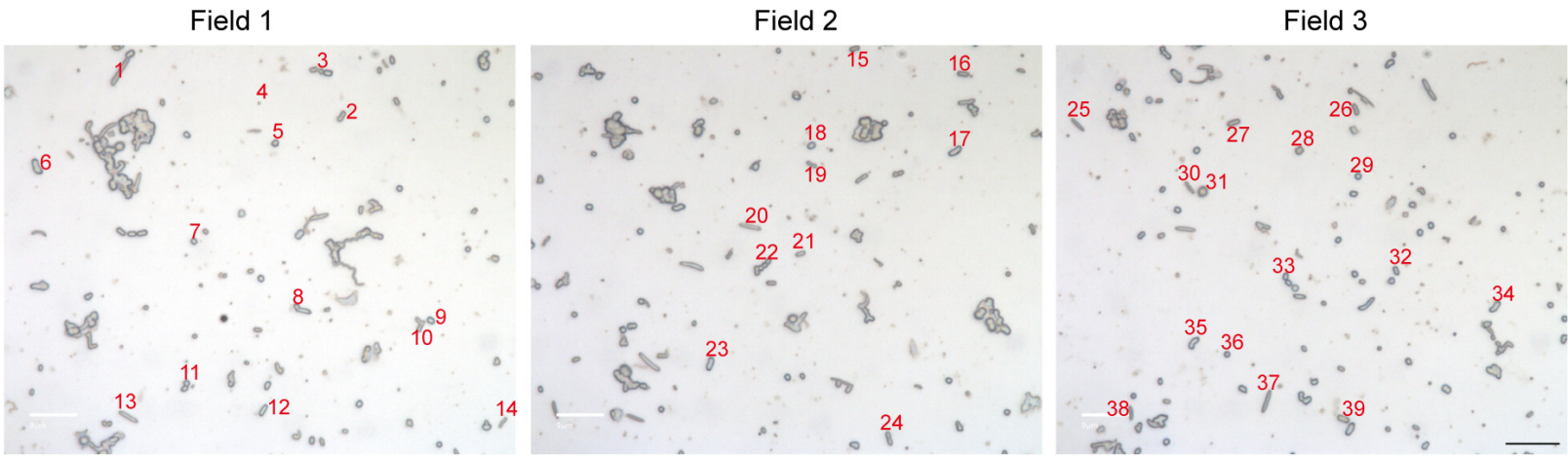
Field 1
Field 2
Field 3

b

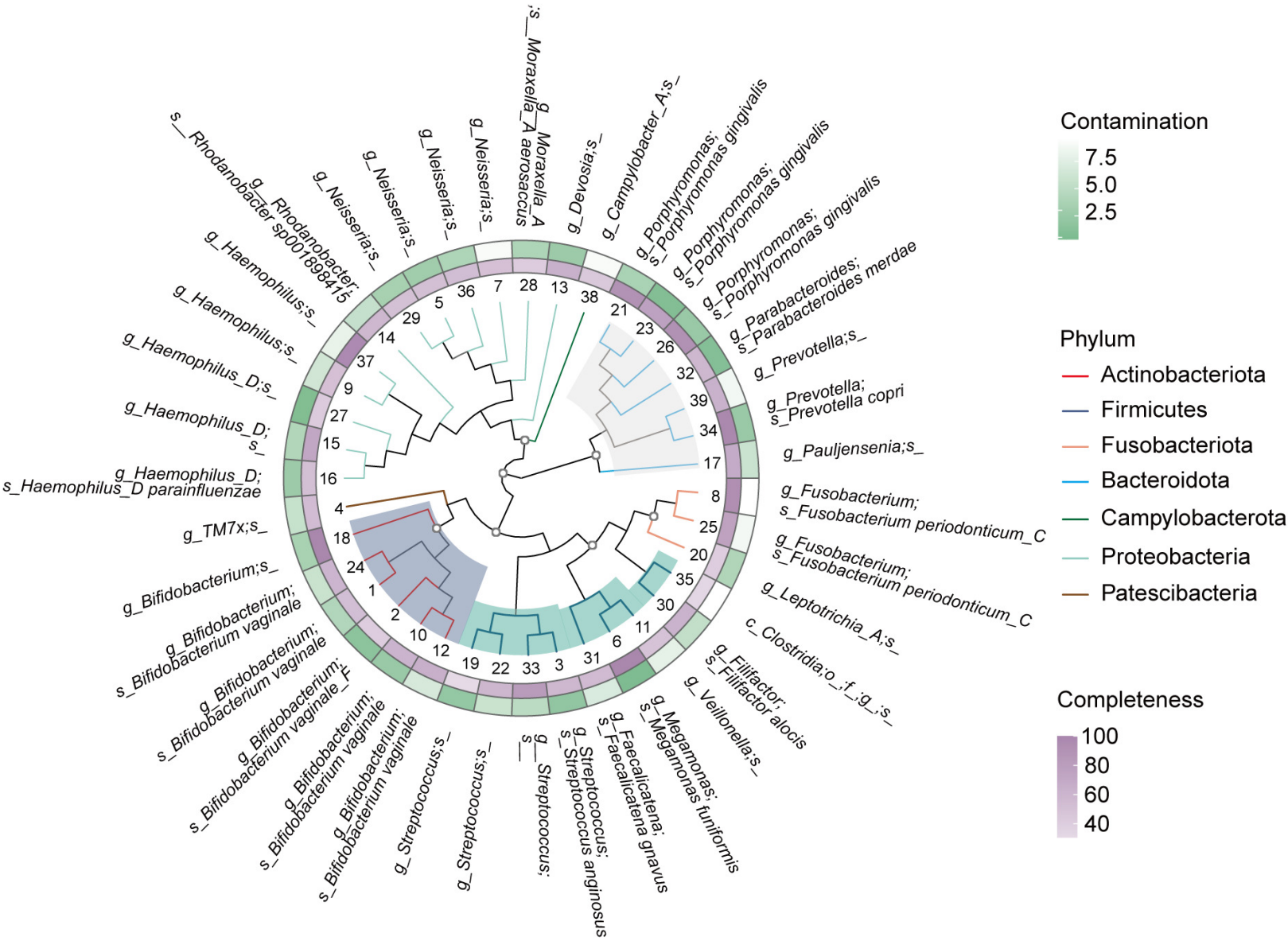
g_Moraxella_A aerosaccus
g_Devosia;s_
g_Campylobacter_A;s_
g_Porphyromonas; s_Porphyromonas gingivalis
g_Porphyromonas; s_Porphyromonas gingivalis
g_Porphyromonas; s_Porphyromonas gingivalis
g_Parabacteroides; s_Parabacteroides merdae
g_Prevotella;s_
g_Prevotella; s_Prevotella copri
g_Pauljensenia;s_
g_Fusobacterium; s_Fusobacterium periodonticum_C
g_Fusobacterium; s_Fusobacterium periodonticum_C
g_Leptotrichia_A;s_
c_Clostridia;o_;f_;g_;s_
g_Filifactor; s_Filifactor alocis
g_Veillonella;s_
g_Megamonas; s_Megamonas funiformis
g_Faecalicatena; s_Faecalicatena gnavus
g_Streptococcus; s_Streptococcus anginosus
g_Streptococcus; s_
g_Streptococcus;s_
g_Streptococcus;s_
g_Bifidobacterium; s_Bifidobacterium vaginale
g_Bifidobacterium; s_Bifidobacterium vaginale
g_Bifidobacterium; s_Bifidobacterium vaginale
g_Bifidobacterium; s_Bifidobacterium vaginale
g_Bifidobacterium;s_
g_TM7x;s_
g_Haemophilus_D; s_Haemophilus_D parainfluenzae
g_Haemophilus_D; s_
g_Haemophilus_D;s_
g_Haemophilus;s_
g_Haemophilus;s_
g_Rhodanobacter; s_Rhodanobacter sp001898415
g_Neisseria;s_
g_Neisseria;s_
g_Neisseria;s_
Contamination
7.5
5.0
2.5
Phylum
Actinobacteriota
Firmicutes
Fusobacteriota
Bacteroidota
Campylobacterota
Proteobacteria
Patescibacteria
Completeness
100
80
60
40

Fig.3

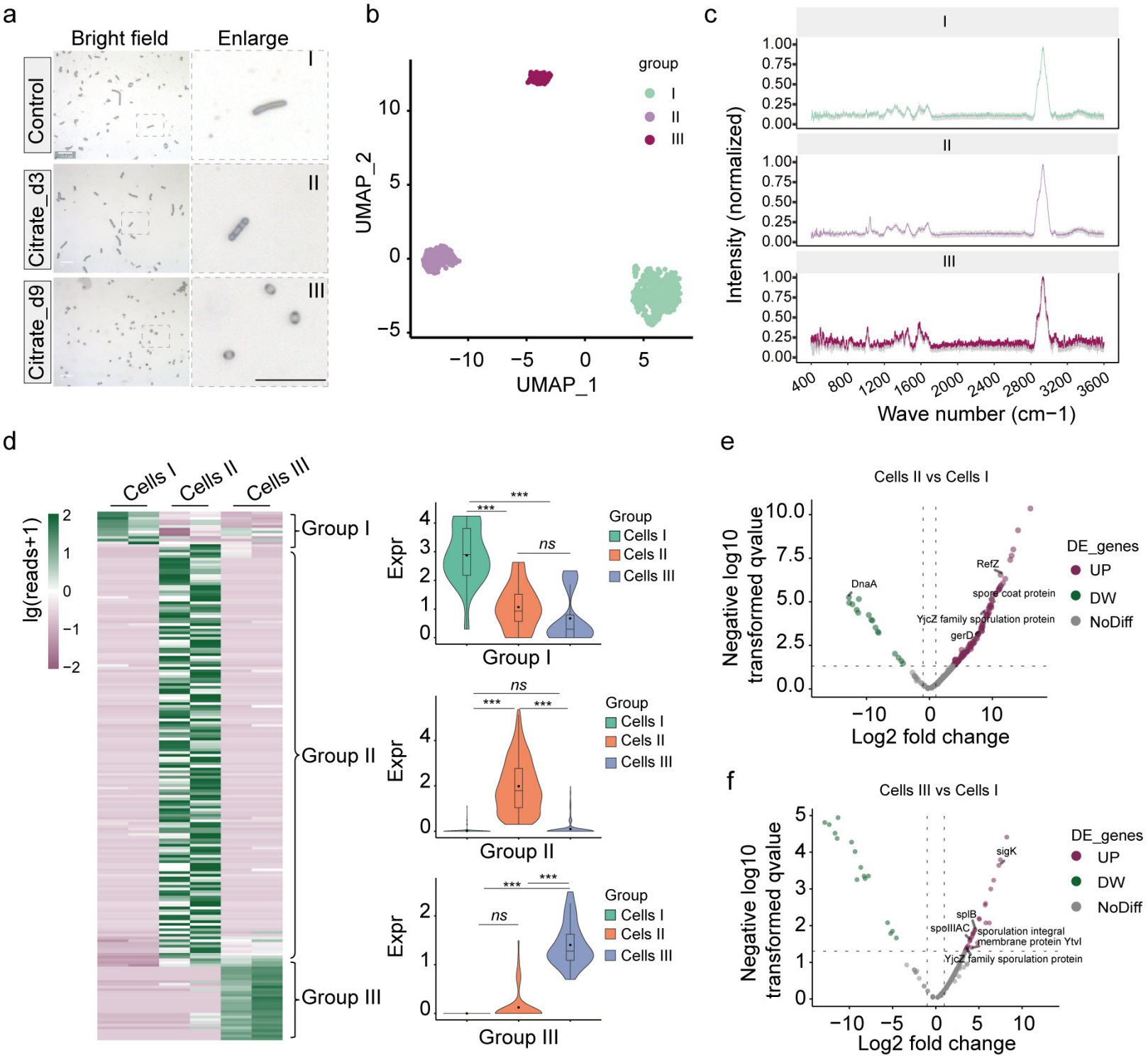
a
Bright field
Enlarge
Control
Citrate_d3
Citrate_d9
I
II
III
b
group
I
II
III
UMAP_2
UMAP_1
c
Intensity (normalized)
Wave number (cm−1)
d
Cells I
Cells II
Cells III
lg(reads+1)
Group I
Group II
Group III
Expr
Group
Cells I
Cels II
Cells III
ns
e
Cells II vs Cells I
Negative log10 transformed qvalue
Log2 fold change
DE_genes
UP
DW
NoDiff
DnaA
RefZ
spore coat protein
YjcZ family sporulation protein
gerD
f
Cells III vs Cells I
sigK
splB
spoIIIAC
sporulation integral membrane protein YtvI
YjcZ family sporulation protein

Fig.4

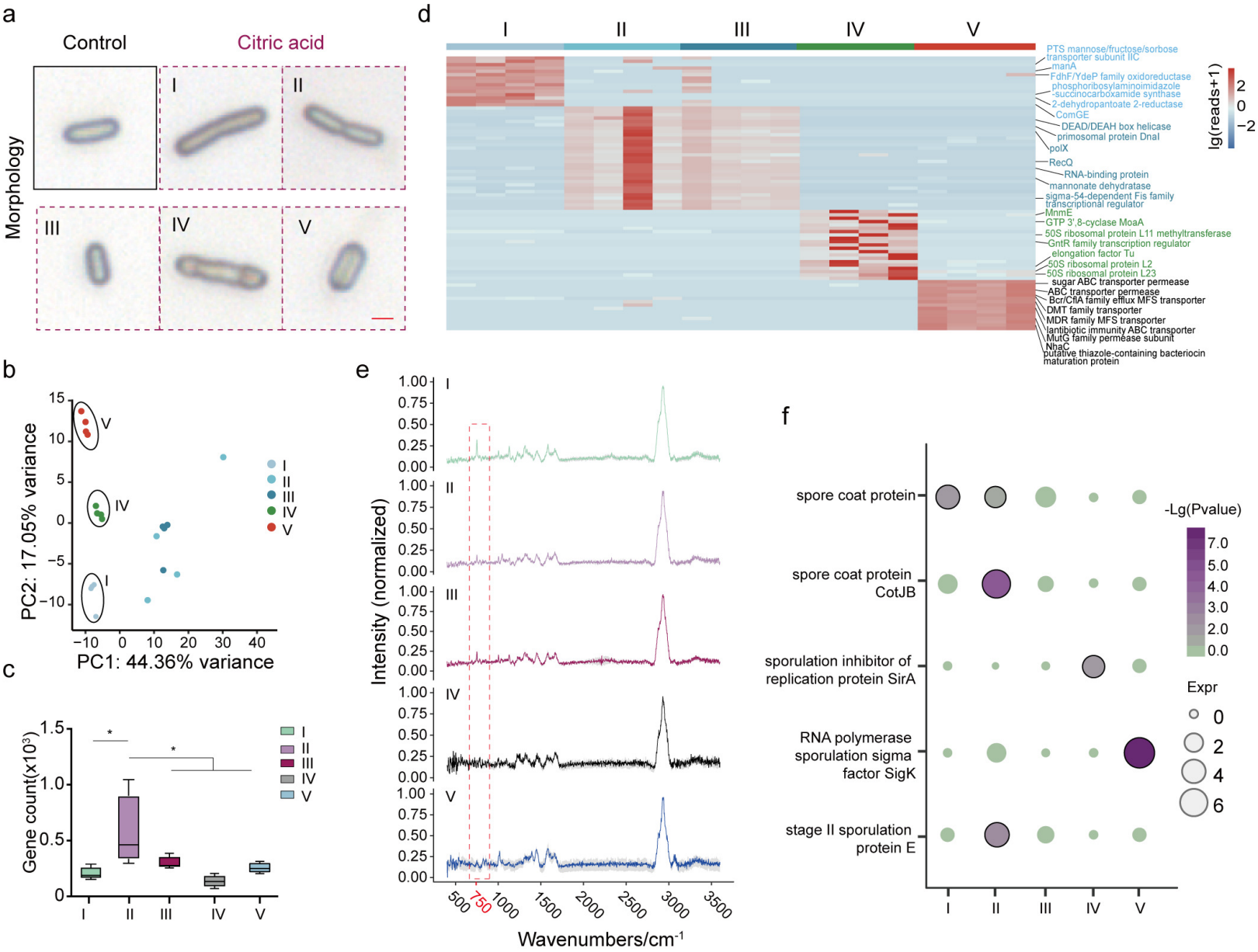
a
Control
Citric acid
Morphology
I
II
III
IV
V
d
lg(reads+1)
PTS mannose/fructose/sorbose transporter subunit IIC
manA
FdhF/YdeP family oxidoreductase
phosphoribosylaminoimidazole-succinocarboxamide synthase
2-dehydropantoate 2-reductase
ComGE
DEAD/DEAH box helicase
primosomal protein DnaI
polX
RecQ
RNA-binding protein
mannonate dehydratase
sigma-54-dependent Fis family transcriptional regulator
MnmE
GTP 3',8-cyclase MoaA
50S ribosomal protein L11 methyltransferase
GntR family transcription regulator
elongation factor Tu
50S ribosomal protein L2
50S ribosomal protein L23
sugar ABC transporter permease
ABC transporter permease
Bcr/CflA family efflux MFS transporter
DMT family transporter
MDR family MFS transporter
lantibiotic immunity ABC transporter
MutG family permease subunit
NhaC
putative thiazole-containing bacteriocin maturation protein
b
PC2: 17.05% variance
PC1: 44.36% variance
c
Gene count(x10³)
e
Intensity (normalized)
Wavenumbers/cm⁻¹
f
spore coat protein
spore coat protein CotJB
sporulation inhibitor of replication protein SirA
RNA polymerase sporulation sigma factor SigK
stage II sporulation protein E
-Lg(Pvalue)
Expr

Fig.5

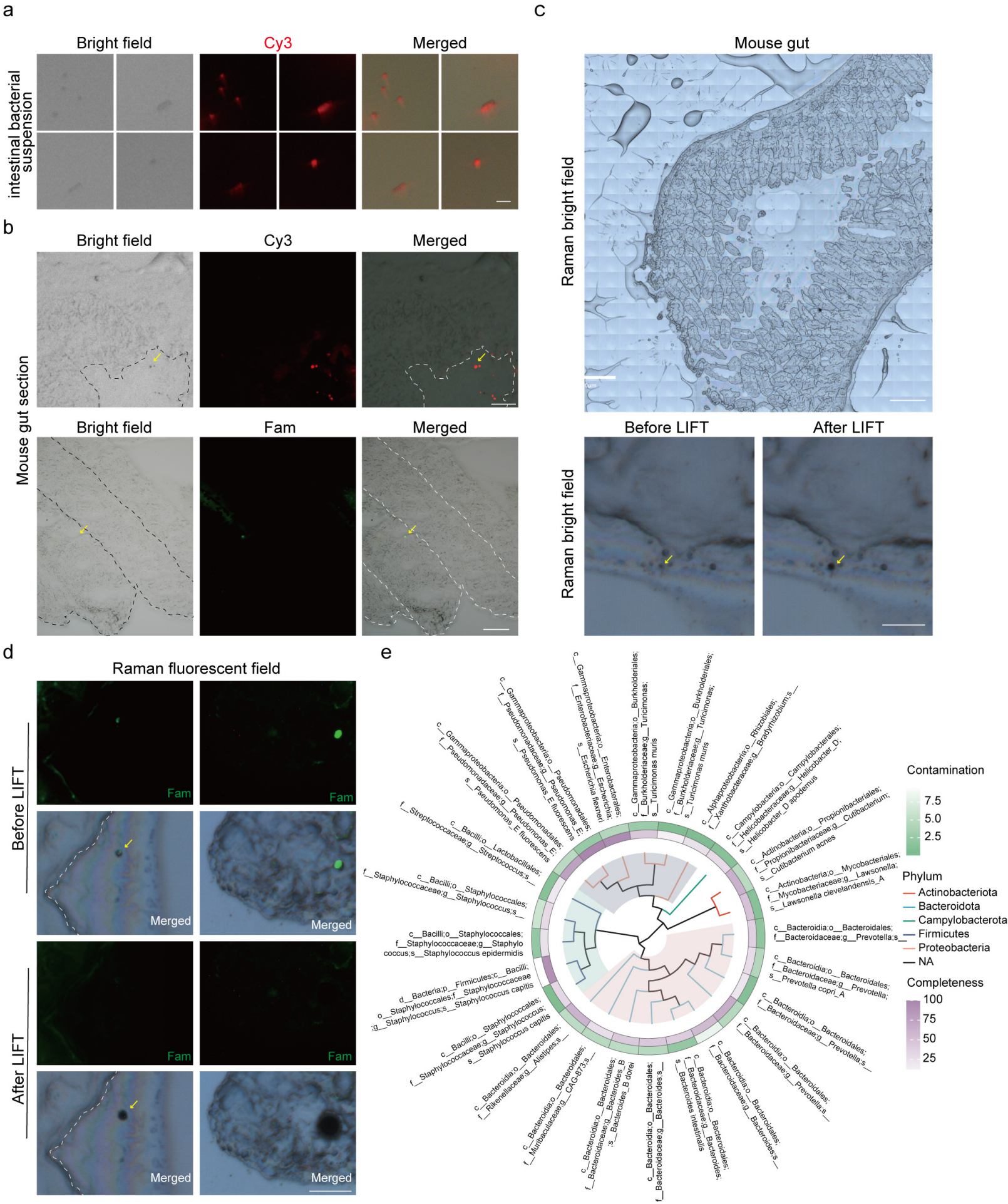
a
Bright field
Cy3
Merged
intestinal bacterial suspension
b
Bright field
Cy3
Merged
Mouse gut section
Bright field
Fam
Merged
c
Mouse gut
Raman bright field
Before LIFT
After LIFT
Raman bright field
d
Raman fluorescent field
Before LIFT
After LIFT
Fam
Merged
e
Contamination
7.5
5.0
2.5
Phylum
Actinobacteriota
Bacteroidota
Campylobacterota
Firmicutes
Proteobacteria
NA
Completeness
100
75
50
25

Fig.6

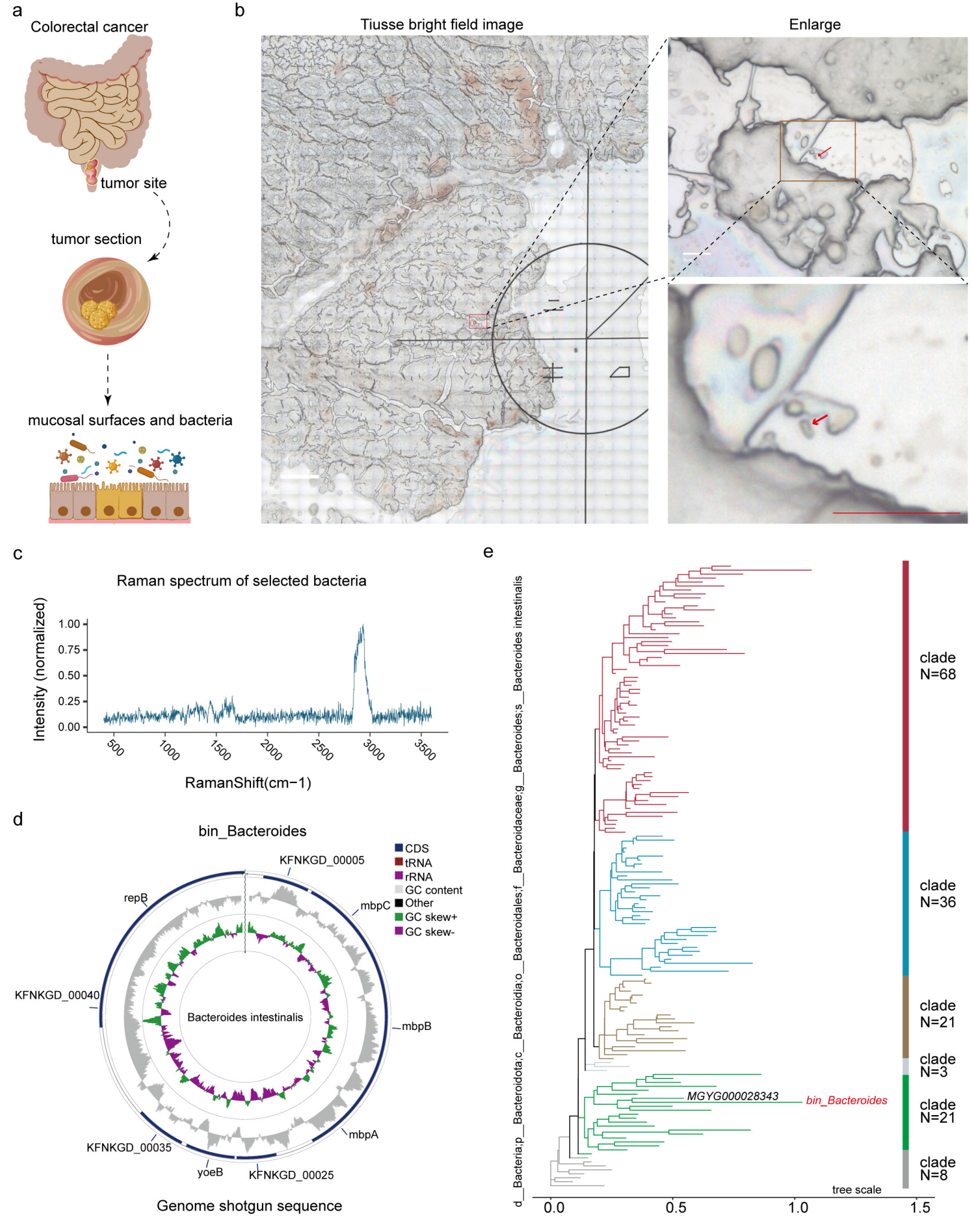
a
Colorectal cancer
tumor site
tumor section
mucosal surfaces and bacteria
b
Tiusse bright field image
Enlarge
c
Raman spectrum of selected bacteria
Intensity (normalized)
1.00
0.75
0.50
0.25
0.00
500
1000
1500
2000
2500
3000
3500
RamanShift(cm−1)
d
bin_Bacteroides
CDS
tRNA
rRNA
GC content
Other
GC skew+
GC skew-
KFNKGD_00005
repB
mbpC
KFNKGD_00040
Bacteroides intestinalis
mbpB
mbpA
KFNKGD_00035
yoeB
KFNKGD_00025
Genome shotgun sequence
e
d__Bacteria;p__Bacteroidota;c__Bacteroidia;o__Bacteroidales;f__Bacteroidaceae;g__Bacteroides;s__Bacteroides intestinalis
clade N=68
clade N=36
clade N=21
clade N=3
clade N=21
clade N=8
MGYG000028343
bin_Bacteroides
tree scale
0.0
0.5
1.0
1.5

Fig.7

a

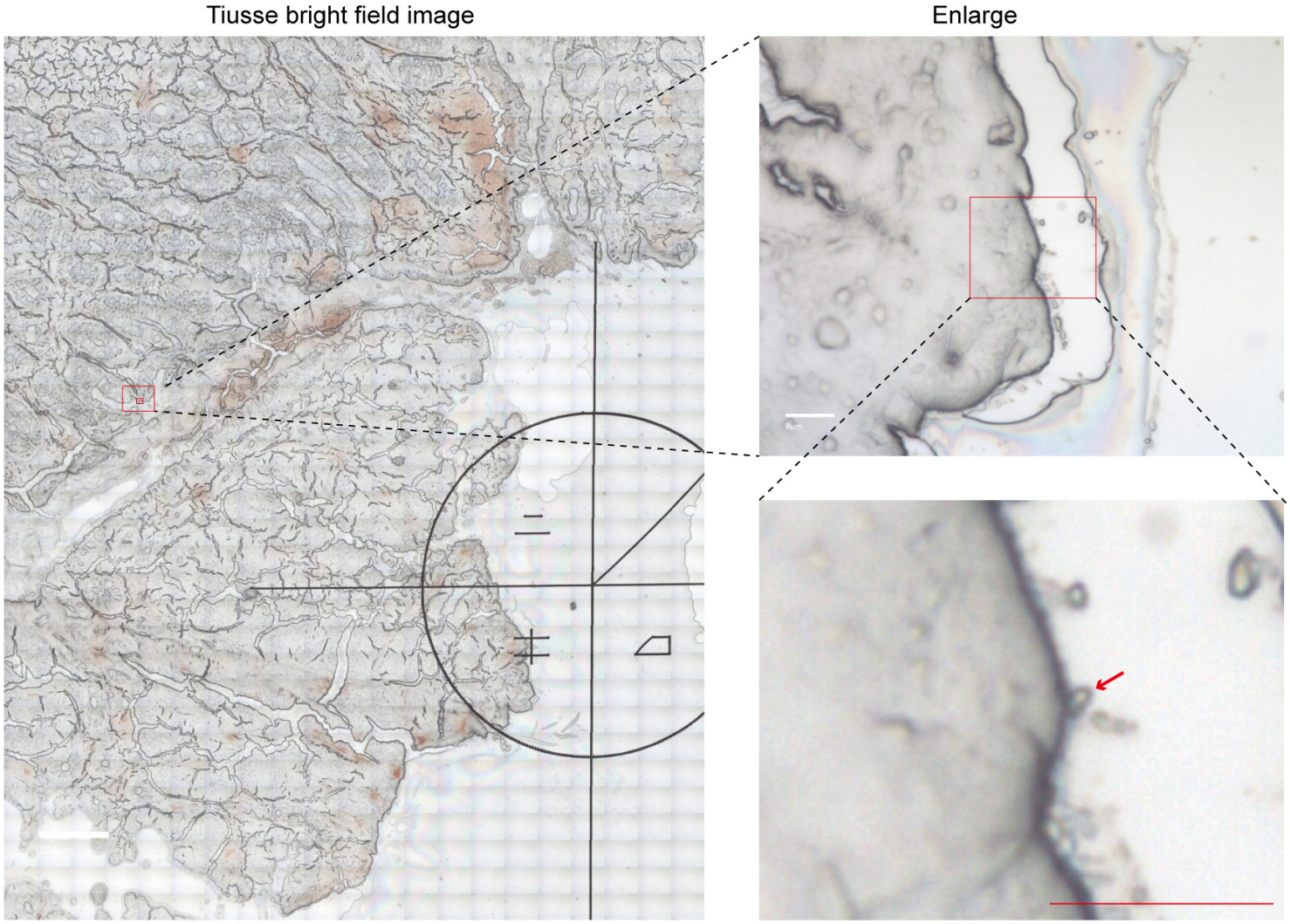
Tiusse bright field image
Enlarge

b

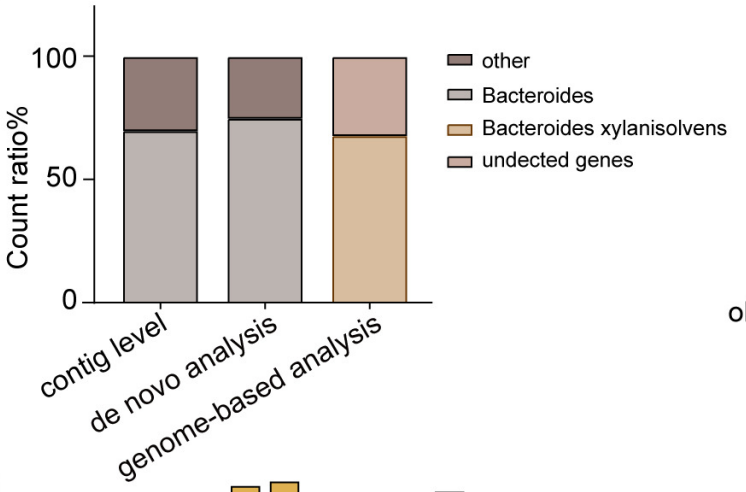
100
50
0
Count ratio%
other
Bacteroides
Bacteroides xylanisolvens
undected genes
contig level
de novo analysis
genome-based analysis

c

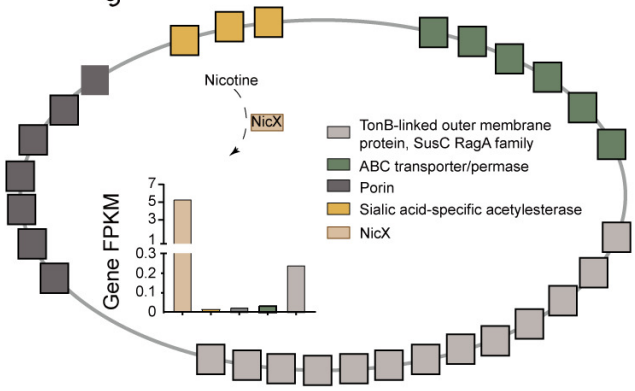
Nicotine
NicX
TonB-linked outer membrane protein, SusC RagA family
ABC transporter/permase
Porin
Sialic acid-specific acetylesterase
NicX
Gene FPKM
7
5
3
1
0.3
0.2
0.1
0

d

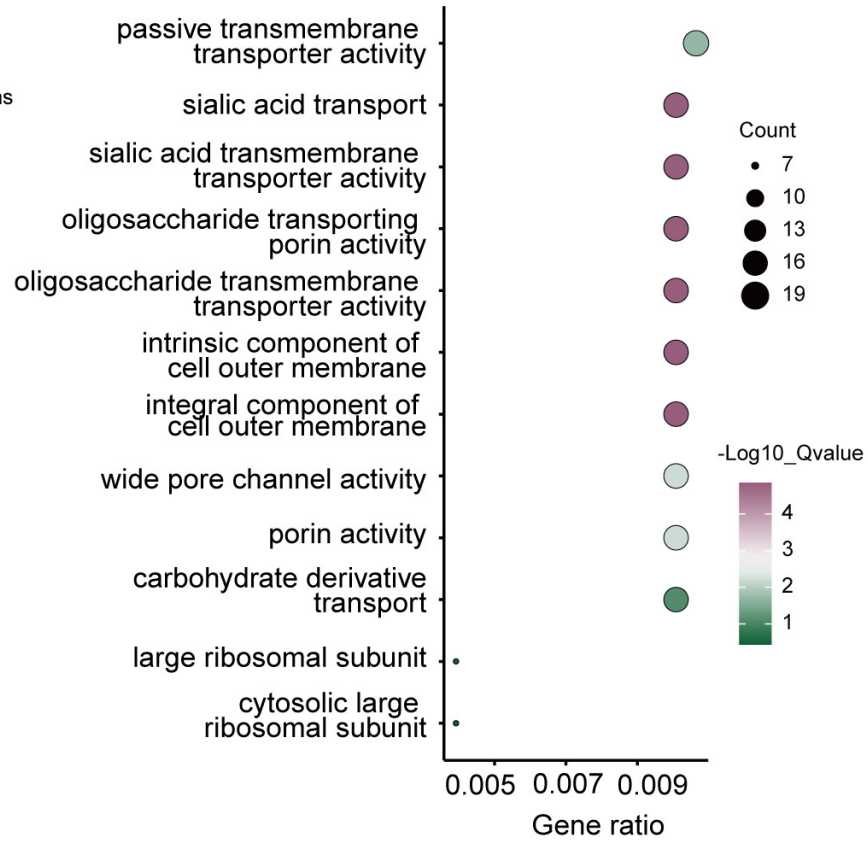
passive transmembrane transporter activity
sialic acid transport
sialic acid transmembrane transporter activity
oligosaccharide transporting porin activity
oligosaccharide transmembrane transporter activity
intrinsic component of cell outer membrane
integral component of cell outer membrane
wide pore channel activity
porin activity
carbohydrate derivative transport
large ribosomal subunit
cytosolic large ribosomal subunit
0.005
0.007
0.009
Gene ratio
Count
7
10
13
16
19
-Log10_Qvalue
4
3
2
1